Journal of Materials Science: Materials in Electronics (2019) 30:491–498
https://doi.org/10.1007/s10854-018-0314-4

Influence of Nd_2O_3/SrO additives on sintering characteristics and microwave dielectric properties of $(Zr_{0.8}Sn_{0.2})TiO_4$ ceramics

Liming Zhang[1,2] · Yi Chang[1,2] · Miao Xin[1,2] · Luchao Ren[1,2] · Xianfu Luo[1,2] · Hongqing Zhou[1,2]

Received: 13 July 2018 / Accepted: 29 October 2018 / Published online: 1 November 2018

Abstract
The phase composition, microstructure, densification, microwave dielectric properties and sintering characteristics of $(Zr_{0.8}Sn_{0.2})TiO_4$ specimens doped with various Nd_2O_3/SrO additions, synthesized via a conventional solid-stated technology, were comprehensively studied. All samples depicted a single uniform $(Zr_{0.8}Sn_{0.2})TiO_4$ phase with orthorhombic crystalline structure without secondary phase. After adding Nd_2O_3/SrO additives, the sintering temperature of ZST ceramics was depressed to 1320 °C, while facilitating dielectric performances, as long as they were added in the appropriate amounts (0.3 wt% Nd_2O_3 + 0.45 wt% SrO). It has been found that when the ZST powders ground for 16 h sintered at 1320 °C for 4 h with 0.3 wt% Nd_2O_3 and 0.45 wt% SrO, an excellent microwave dielectric performances were generated for sintered ceramics: $\varepsilon_r = 40.61$, $Q \times f = 40700$ GHz (f = 5.5 GHz) and $\tau_f = -2.57$ ppm °C^{-1}.

1 Introduction

Along with the advancements of microwave communication technique, dielectric ceramics have been extensively used in wireless systems such as cellular mobile, driverless systems, passive components, and thin-film substrates [1–3]. Especially, the materials with high permittivity, good quality factor, and near-zero temperature coefficient of the resonant frequency can achieve the purpose of miniaturization of the installations, high-speed conversion of electronic signals at ultra-high frequency and the stability of resonant frequency [4–7].

From the point of previous investigations, $(Zr_{0.8}Sn_{0.2})TiO_4$ ceramics have drawn attention to tremendous interests all over the world for its high dielectric constants ($\varepsilon_r \geq 25$), high quality factor ($Q > 5000$) and near-zero temperature coefficient of the resonant frequency ($\tau_f < \pm 10$ ppm/°C). However, the pure $(Zr_{0.8}Sn_{0.2})TiO_4$ ceramics require extra high sintering temperature (> 1400 °C) to be densification, which depresses its practicability to a great extent [8–10]. A number of published articles have mentioned that ZST ceramics could be modified by adding some oxide additions such as Nd_2O_3, La_2O_3, Fe_2O_3, CuO and SrO etc. [11–13]. These oxide additions in appropriate amounts not only depressed the sintering temperature of ZST ceramics, but also optimized the dielectric performances, effectively, and as a result, practical application of ZST ceramics was extensively expended. Pamu et al. [11] added 0.5 wt% Nd_2O_3 + 1 wt% ZnO into ZST forming a specimen with good overall properties of $\rho = 5.05$ g/cm^3, $\varepsilon_r = 40$, $Q \times f = 59{,}300$ GHZ and $\tau_f = -3$ ppm °C^{-1}. Chen et al. [14] showed ZST specimens mixed with 0.5 wt% CaO + 1 wt% La_2O_3 displayed optimal dielectric performances of $\varepsilon_r = 39.56$ and $Q \times f = 44{,}100$ GHz, $\tau_f = -1.66$ ppm °C^{-1}. Zhang et al. [15] synthesized the ZST specimens with 1 wt% La_2O_3 + 2 wt% BaO, and exhibited synthetical performances of $\varepsilon_r = 41$, $Q = 9800$, and $\tau_f = -3.79$ ppm °C^{-1}. Pamu et al. [13] depressed the sintering temperature of the ZST specimens to 1350 °C by adding 0.5 wt% SrO + 1 wt% ZnO, with dielectric performances of $\varepsilon_r = 37$, and $Q \times f = 54{,}250$ GHz (f = 11.94 GHz), $\tau_f = 6.2$ ppm °C^{-1}. It can be found that the addition of divalent metals and trivalent rare earth element oxides did have a great influence on the sintering characteristics and dielectric performances of ZST ceramics [16, 17]. Nevertheless, adding the compound additives of Nd_2O_3/SrO to ZST ceramics has not been researched. In the following report, we comprehensively exhibited the influence of Nd_2O_3/SrO additions on the crystal structure, sintering characteristic, densification and dielectric performances of ZST

✉ Hongqing Zhou
hqzhou@njtech.edu.cn

[1] College of Materials Science and Engineering, Nanjing Tech University, Nanjing 210009, China

[2] Jiangsu Collaborative Innovation Center for Advanced Inorganic Function Composites, Nanjing 210009, China

ceramics. Furthermore, effects of particle size on dielectric performances of sintered specimens were also studied.

2 Experimental procedure

The powders were prepared via the traditional solid-phase synthesis technology from the raw materials of ZrO_2 (> 99.9%, D50 = 0.626 μm), SnO_2 (> 99.9%, D50 = 0.489 μm), and TiO_2 (> 99.9%, D50 = 0.497 μm). These oxides were mingled uniformly in the distilled water, using the roll mill, according to the required stoichiometry composition of $(Zr_{0.8}Sn_{0.2})TiO_4$. After drying, the mixtures were calcined at 1150 °C for 2 h in air atmosphere. Then the ZST powders (D50 = 4.212 μm) were obtained after being ground by ZrO_2 balls for 5 h. In addition, for studying the influence of particle size, the ZST powders were also milled for 4, 8, 12, 16, 20, 24 h. SrO powders were synthesized by calcining $SrCO_3$ (> 99.9%, D50 = 0.984 μm) materials at 1150 °C for 5 h. In this study, the proportion of Nd_2O_3 (> 99.9%, D50 = 1.336 μm) and SrO was controlled at 1:1.5. The weight percent of Nd_2O_3/SrO additives and the serial numbers were shown in Table 1. The calcined ZST powders mixed with desired amounts of Nd_2O_3/SrO were pressed into 13.4 mm diameter, 7–8 mm height cylinders at 120 MPa after adding 10 wt% of an 8% solution of PVA and being pelleted. The cylinders were ultimately sintered at diverse temperatures ranging from 1260 to 1380 °C for 4 h in the air atmosphere, with a temperature rise speed of 120°C/h and cooling rate of 60 °C/h [18].

The Archimedean immersion method was used to confirme the sintered density of the ZST specimens. Crystal structure of sintered ZST specimens analyzed by technique of XRD ($20° \le 2\theta \le 70°$, $10° \text{ min}^{-1}$) [19]. The microstructure of sintered samples was represented and identified via virtue of a scanning electron microscope (SEM, JEOL, JSM-5900). The average particle size of all testing powders was measured by a laser particle size analyzer (Model 3500, Microtrac, Largo, FL, USA). Flexure strength of all measured samples (3 mm × 5 mm × 60 mm^3) was determined using three-point bending means in accordance with RGWT-4002 via a conventional testing equipment in air. The dielectric constant (ε_r) and unloaded Q factor at microwave frequencies were examined by the Hakki–Coleman dielectric resonator technique, using a network analyzer. The temperature coefficient of the resonant frequency (τ_f) was obtained via testing the resonant frequency from 25 to 80 °C. The formula for calculating the τ_f is as follows:

$$\tau_f = \frac{1}{f_{25}} \times \frac{f_{80} - f_{25}}{80 - 25}, \quad (1)$$

where f_{25} and f_{80} represent the resonant frequency at 25 °C and 80 °C, severally.

Table 1 Weight percent of additives in ZST ceramics

Sample designation	Nd_2O_3 (wt%)	SrO (wt%)	Total additives (wt%)
NS075	0.3	0.45	0.75
NS150	0.6	0.9	1.5
NS225	0.9	1.35	2.25
NS300	1.2	1.8	3.0

3 Results and discussion

3.1 Structural analysis

Figure 1 demonstrated the XRD diagrams of ZST specimens doped with various weight percent of Nd_2O_3/SrO additions sintered at 1320 °C for 4 h. The tagged peaks exhibited a uniform phase with α-PbO_2 orthorhombic structure belonging to the space group D142h = Pbcn. All samples showed no secondary phase under the detection of different intensities because the second-phase was too minor to be detected by X-ray diffraction [11, 15]. In order to investigate the doping mechanism of sintered samples, the main peaks (111) of specimens were amplified in Fig. 1b. As we could find, the dominant diffraction peaks approached to a low diffraction angle with the increase of Nd_2O_3/SrO additions. Furthermore. the lattice parameters a_0, b_0, c_0 and unit cell volume V_0, received by calculating according to these peaks, were presented in Table 2. The unit cell volume of specimens expanded generally as the Nd_2O_3/SrO additions increased. These results were mainly attributed to the difference among the tetravalent ions and replacement ions in sintered specimens. To be specific, according to the Bragg equation ($2d\sin\theta = n\lambda$) that relationship between the diffraction angle and interplanar spacing is inversely proportional, the substitution ions Nd^{3+}, Sr^{2+} radius of 0.983 Å and 1.18 Å are much larger than the tetravalent ions Zr^{4+}, Sn^{4+}, Ti^{4+} radius of 0.72 Å, 0.69 Å, and 0.61 Å [20]. Hence, the increase of Nd_2O_3/SrO additions amplified the interplanar space, and enlarged the unit cell subsequently, which was also agree with the phenomenon that the main diffraction peaks shifted to a lower angle in Fig. 1b.

3.2 Scanning electron microscopy analysis

Figure 2a–d depicted the SEM micrographs of ZST specimens doped with various weight percent of Nd_2O_3/SrO additions sintered at 1320 °C. We observed that the grain for NS075 was well-developed and homogeneous, and the typical microstructure was dense with few microcracks in

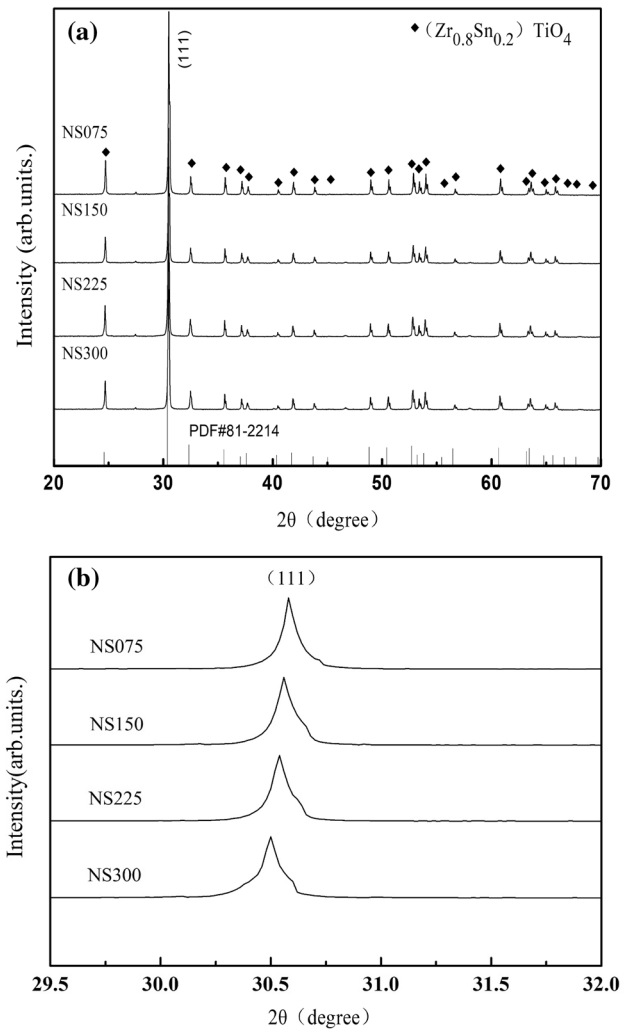

Fig. 1 X-ray diffraction of Nd_2O_3/SrO doped ZST ceramics with different amounts sintered at 1320 °C

Table 2 Calculated unit cell parameters and unit cell volume for ZST ceramics

Composition	Sintering Temperature (°C)	Lattice parameters			Unit cell volume, V_0 (Å^3)
		a_0 (Å)	b_0 (Å)	c_0 (Å)	
NS075	1320	0.4833	0.5424	0.4947	129.68
NS150	1320	0.4791	0.5501	0.5042	132.88
NS225	1320	0.4722	0.5575	0.5098	134.21
NS300	1320	0.4713	0.5612	0.5147	136.14

Fig. 2a, since the adequate liquid phase could provide a faster transmission route to make the process of grains rearrangement and densification more quickly. Hence, the grain growth was improved ultimately [21]. However, the homogeneity of grain size for sintered specimens was degraded with the increase of Nd_2O_3/SrO additives attributed to the superfluous liquid phase and high surface energy, which resulted in the worsen of the densification process and limitation of grain growth. Figure 2e, f showed the representative microstructure of fractured surfaces for NS075 sintered at various temperature. Compared with NS075 sintered at 1320 °C, the grain sintered at 1260 °C was not fully developed and the grain size was smaller than normal since the temperature of 1260 °C was not enough to form sufficient force to make the ceramics densify and restrain the elimination of holes, as a result, increasing intragranular porosity in the ceramics [22]. Overhigh sintering temperature (1380 °C) led to the appearance of larger holes and the abnormity for grain growth. To sum up, the great densification, well-developed grain, and homogeneous microstructure of ceramics required the appropriate amounts of additives.

3.3 Bulk density

Figure 3 illustrated the sintered density of specimens doped with different amounts of Nd_2O_3/SrO additions sintered at diverse temperatures. The sintered density of ZST samples depressed evidently at the same temperature, with increase of Nd_2O_3/SrO additives. Furthermore, the sintered density of all ZST specimens initially increased, and then dropped as the sintering temperature increased, reaching a peak value for all the samples at 1320 °C, thus we determined that the sintering temperature (1320 °C) was the optimal point. Contrasted with theoretical density of pure ZST ceramics (5.19 g cm^{-3}), the sintered specimens sintered at 1320 °C achieved the optimal bulk density of 5.15 g cm^{-3} (99.17%), 5.12 g cm^{-3} (98.63%), 5.08 g cm^{-3} (97.89%), and 5.03 g cm^{-3} (96.91%) for NS075, NS150, NS225, and NS300, respectively. The maximum sintered density may have appeared due to the scarcity of microcracks, close arrangement of the grains and decrease of the grain boundary area. Figure 2a showed the few pores, well-developed grains and homogeneous microstructures, which made the ceramics fully dense, and reached the best optimal value. The samples with large amounts of additives showed the relative low bulk density due to the intergranular porosity, heterogeneous grain size and the excessive liquid phase, as shown in Fig. 2d. Compared with pure ZST ceramics (densification at 1600 °C), appropriate additives of Nd_2O_3/SrO could provide advisable liquid phase promoting the process of densification at lower temperature, while improving the microstructures.

3.4 Dielectric performances

Figure 4 investigated the permittivity of ZST specimens with various weight percent of Nd_2O_3/SrO additions sintered at different temperatures. Compared with four groups

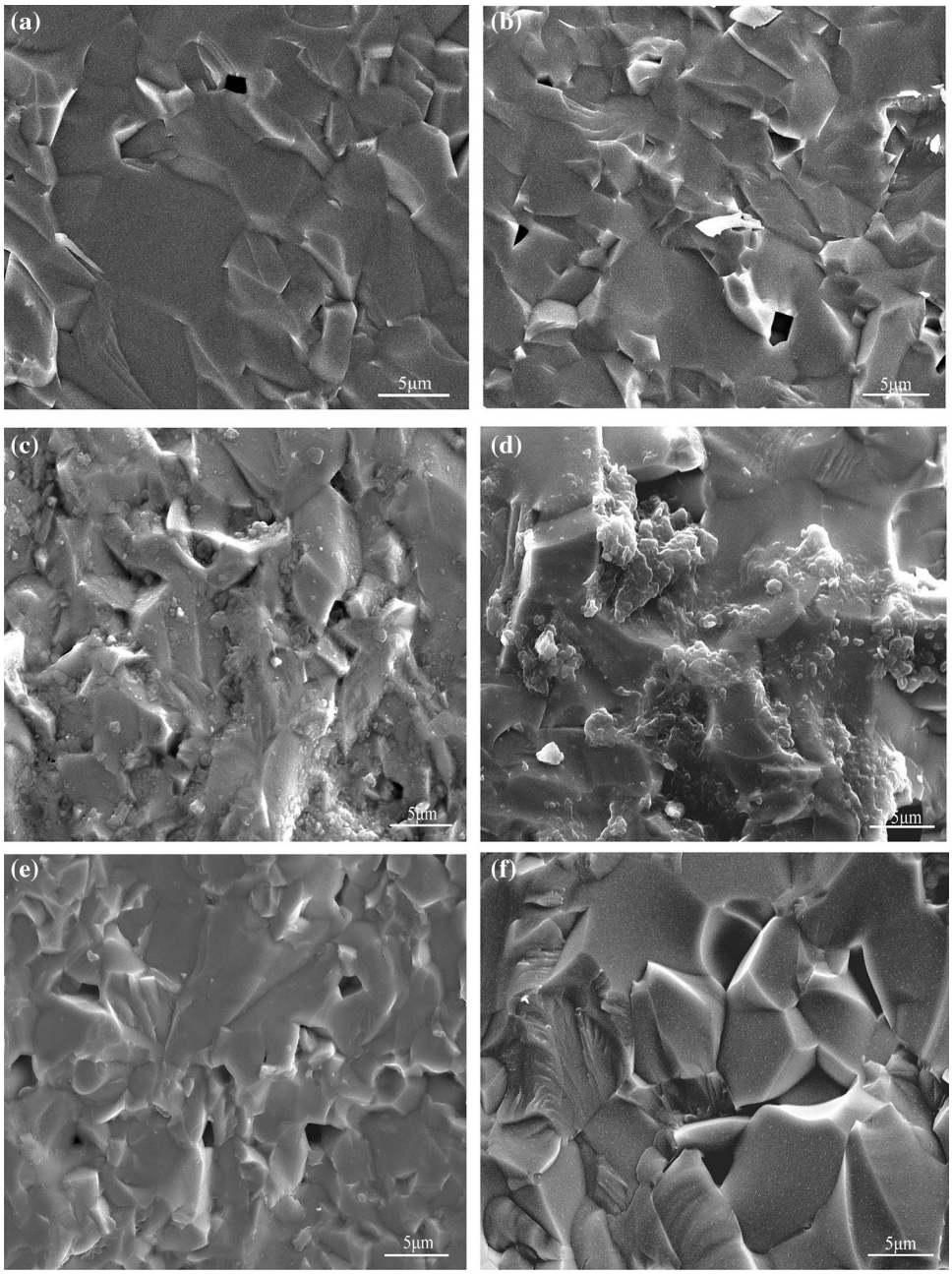

Fig. 2 SEM micrographs on fractured surfaces of ZST ceramics with **a** NS075, **b** NS150, **c** NS225, **d** NS300 sintered at 1320 °C, **e** NS075 sintered at 1260 °C, **f** NS075 sintered at 1380 °C

of sintered ceramics in Fig. 4, we observed that the permittivity mostly declined with the increase of Nd_2O_3/SrO additions. Besides, for the same sample, as the sintering temperature increasing, the permittivity firstly increased and subsequently decreased after reaching a best optimal value at 1320 °C. The maximum value of 40.24 for NS075 was achieved at 1320 °C, and we found that the maximum density was also obtained at this point. It was reported that sintered densities, element compositions, crystalline structures, and secondary phase in the ceramics determined the dielectric permittivity [23]. In previous study, the ZST ceramics sintered at various temperatures exhibited no secondary phase and no structure transformation, and therewith the bulk density became the determining factor of dielectric constants. According to Clausius–Mossotti equation, it is widely believed that the permittivity is affected by the whole dielectric polarizability in the molecule and molar volume [24]. Therefore, when the bulk density of sintered ZST specimens increased, more dipoles participated in polarization per unit volume, and promoted the dielectric constants. Furthermore, the additives of Nd_2O_3/SrO could improve the ionic polarizabilities of ZST ceramics, which was attributed to the fact that Nd^{3+} (5.01 $Å^3$) ion and Sr^{2+} (4.24 $Å^3$) ion exhibit higher dielectric polarizabilities than

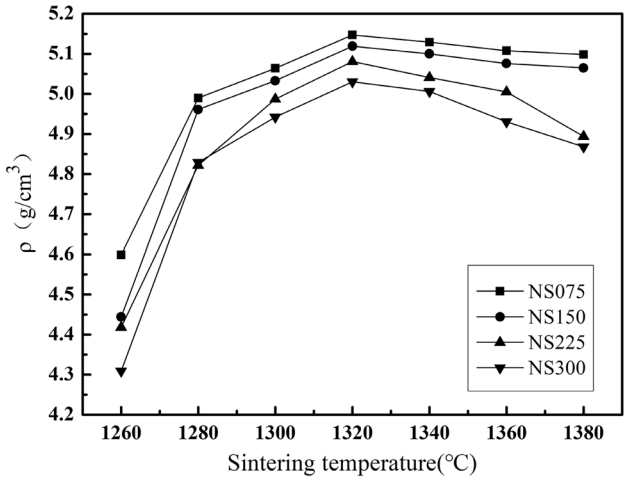

Fig. 3 Bulk densities (ρ) of ZST ceramics with different amounts of Nd_2O_3/SrO additives as a function of sintering temperature

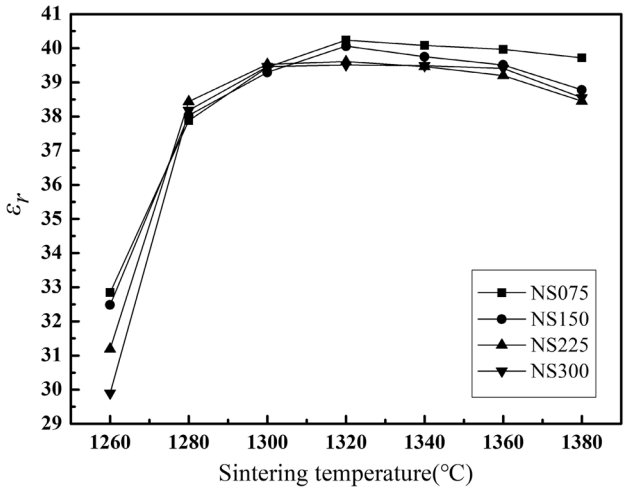

Fig. 4 Dielectric constants (ε_r) of ZST ceramics doping with different amounts of Nd_2O_3/SrO additions at different temperatures

Zr^{4+} (3.25 Å^3) ion, Sn^{4+} (2.83 Å^3) ion, and Ti^{4+} (2.93 Å^3) ion [25]. However, the increase of the unit cell volume V_0 (Table 2) led to the expansion of the oxygen octahedron in the ZST ceramics, resulting in the decline of dielectric polarizability, which caused the depression of permittivity of ZST ceramics, ultimately.

Figure 5 showed the quality factor (Q×f) value of specimens doped with diverse mass percent of Nd_2O_3/SrO additions sintered at different temperatures. We observed the Q×f value of specimens primely elevated with the increase of sintering temperature and declined since receiving an optimal value of 39,720 GHz for NS075 at 1320 °C. The lattice vibration modes, extended dislocations, grain growth, densification, intragranular porosity, phase compositions and vacancies made a big difference in determination of

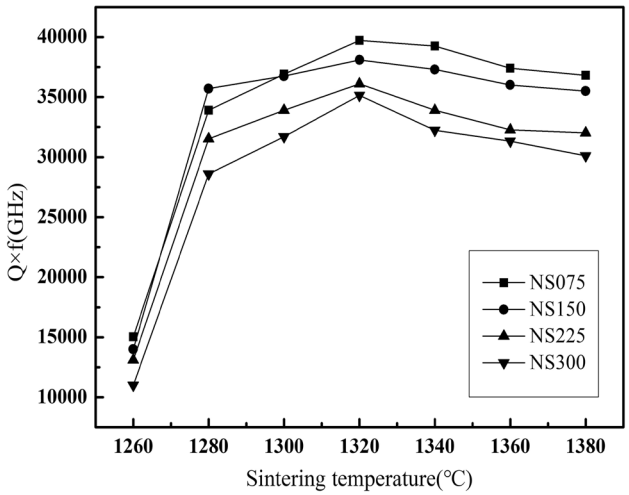

Fig. 5 Q×f values of Nd_2O_3/SrO doped CTSA ceramics with various amounts additions sintered at different temperature

microwave dielectric loss [26]. Overall, the fluctuation trend of the Q×f value was consistent with the variation of bulk density shown in Fig. 3, which also seemed to indicate that densification had a significant influence on the dielectric loss of ZST ceramics. In addition, the crystal boundaries possibly degraded the quality factor of ZST specimens because of plane defects. The ZST ceramics for NS075 depicted in Fig. 2a showed the large and homogenous grain morphology, leading to decreasing the area of grain boundary, causing the reduction of the lattice defects, thereby obtaining a high quality factor [27]. The dielectric loss of specimens was likely to be influenced by the oxygen entrance to the microstructure since any addition of trivalent impurity in the structure increased the oxygen vacancies [28]. To be specific, Nd^{3+} ion served as an acceptor in ceramics, and more oxygen vacancies appeared in microstructures with the increase of Nd_2O_3/SrO additions, which raised the intensity of anharmonic interaction, depressing the quality factor value of ZST ceramics finally. The reaction occurred in microstructures shown as follow:

$$Nd_2O_3 \rightarrow 2Nd'_{Ti} + 3O_o + \ddot{V}_o \quad (2)$$

Figure 6 depicted the average particle size of ZST powders with various milling time. With the increase of zirconia ball grinding time, the average particle size of ZST powders constantly declined, and the mechanical energy was effectively converted into the specific surface energy of the powders. Figure 7 exhibited the permittivity (ε_r) and quality factor (Q×f) value for NS075 with various milling time of ZST powders. Clearly, as the milling time increased from 4.0 to 16 h, the permittivity increased from 40.18 to 40.61 and the quality factor values from 39,600 to 40,700 GHz. Nevertheless, after further increasing the milling time, the dielectric

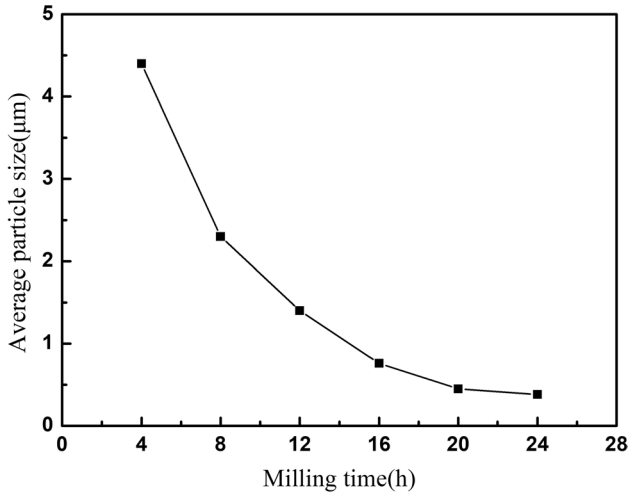

Fig. 6 Average particle size of ZST powders with various milling time

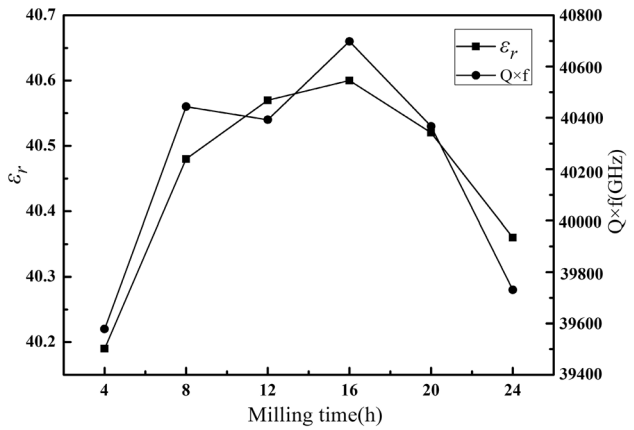

Fig. 7 Dielectric constants (ε_r) and Q×f values for NS075 as a function of milling time

performance of ZST ceramics was evidently reduced. In the sintering process dominated by liquid-phase sintering, the powders with appropriate ball milling time had high specific surface energy, and better powder activity, which could provide a greater driving force for liquid-phase transmission, grain growth, particle rearrangement and the dissolution and precipitation to improve the densification [29, 30]. The further promotion of quality factor was also attributed to the good particle size distribution, as depicted in Fig. 8, facilitating the tight combination of grain in the sintering process. However, the excessive milling time resulted in the destruction of crystal structure, increase of plane defects mentioned above, and risen of unsaturated position and charged structural units on the surface of powders, deteriorating the quality factor [31, 32].

For the purpose of further investigating the effects of particle size on dielectric properties, Fig. 9a, b depicted

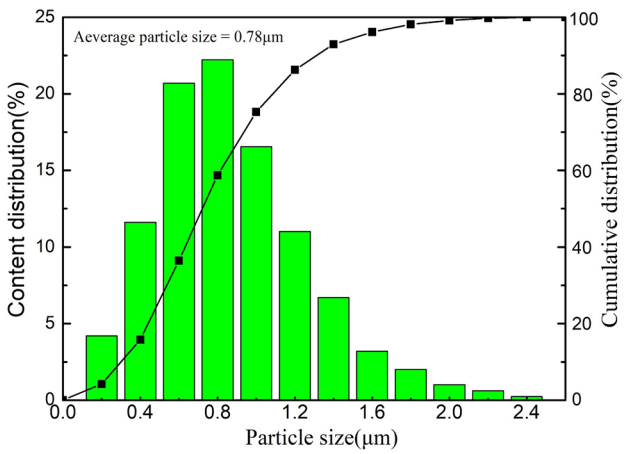

Fig.8 Particle size distribution of ZST powders after milling for 16 h

the SEM micrographs of ZST powders of different milling times doped with 0.3 wt% Nd_2O_3 + 0.45 wt% SrO sintered at 1320 °C. Compared with Fig. 2a, the grains were arranged more closely so that there were almost no pores, minimizing the grain boundary area, as exhibited in Fig. 9a. In the above report, we have mentioned that depressing the grain boundary area could effectively reduce the dielectric loss and improve the quality factor. Nevertheless, when the milling time was excessive, the porous microstructure was observed in Fig. 9b, and the grain boundary area increased evidently, leading to the degradation of dielectric performances. In general, the particle size did have a significant effect on the dielectric properties of sintered specimens.

Table 3 demonstrated the influence of different additives on the sintered density, permittivity, quality factor, and flexure strength of four representative ZST specimens. The τ_f of ZST specimens were −2.55, −3.13, −3.34, and −3.51 ppm $°C^{-1}$ for NS075, NS150, NS225, and NS300 sintered at 1320 °C, separately. We observed that τ_f was quite stable, meaning that these ceramics had a good temperature stability of dielectric constants at 25–80 °C. Besides, we found that the effect of particle size on temperature coefficient was slight, which attributed to the fact that the temperature coefficient of the resonant frequency under the microwave frequency is mainly dominated by the components and the secondary phases existing in the ceramics [24]. As it was clearly to see, with the increase of Nd_2O_3/SrO additions, the flexure strength of samples dropped sharply from 103.88 to 74.62 MPa. Compared ZST ceramics mingled with other elements shown in Table 3, Nd_2O_3/SrO additives could depress the sintering temperature to 1320 °C and promote the bulk density to 5.15 g cm^{-3}, positively. NS075 (16 h) likely turns into the promising option for microwave communication application attributed to its low sintering temperature of 1320 °C, excellent dielectric constant of 40.61, high quality

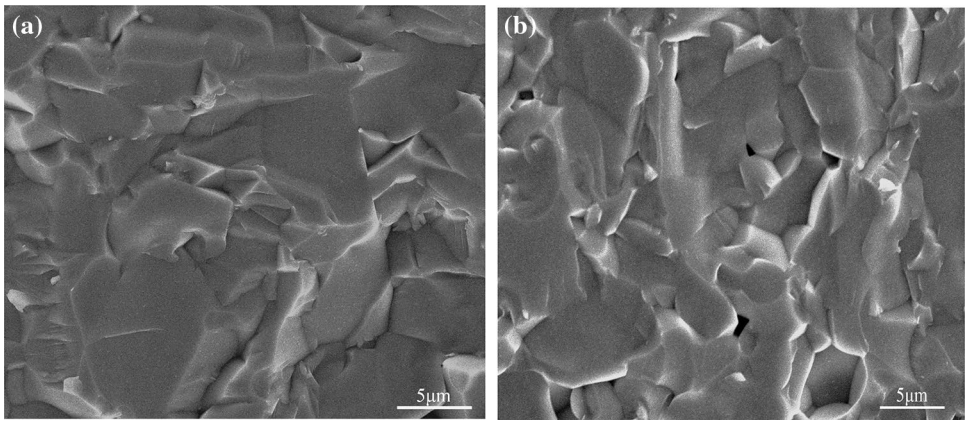

Fig. 9 SEM micrographs of ZST powders of different milling times, **a** 16 h, **b** 24 h, doped with 0.3 wt% Nd_2O_3 + 0.45 wt% SrO sintered at 1320 °C

Table 3 Bulk densities, dielectric properties and flexure strength of ZST ceramics with different additives

Compositions	Sintering temperature (°C)	ρ (g cm^{-3})	ε_r	Q	τ_f (ppm °C^{-1})	Flexure strength (MPa)
Pure ZST [16]	1600	4.92	36.10	7000	0	–
0.5 wt% Nd_2O_3 + 1.0 wt% ZnO [11]	1400	5.05	40.00	4930	− 3.00	–
0.5 wt% SrO + 1.0 wt% ZnO [13]	1350	5.02	37.00	4500	+ 6.20	–
1.0 wt% La_2O_3 + 0.5 wt% CaO [14]	1335	5.06	39.56	7875	− 1.66	
1.0 wt% La_2O_3 + 2.0 wt% BaO [15]	1350	5.10	41.00	9800	− 3.79	–
NS075	1320	5.14	40.24	7200	− 2.55	103.88
NS150	1320	5.12	40.06	6900	− 3.13	89.98
NS225	1320	5.08	39.61	6500	− 3.34	85.65
NS300	1320	5.03	39.51	6400	− 3.51	74.62
NS075 (16 h)	1320	5.15	40.61	7400	− 2.57	103.92

factor of 7400 (f = 5.5 GHz), and near-zero temperature coefficient of the resonant frequency, − 2.57 ppm °C^{-1}.

4 Conclusions

The microstructure and dielectric performances of ZST specimens double-doped with Nd_2O_3 and SrO have been comprehensively investigated. The secondary phase was not detected from the X-ray diffraction pattern. It has been found that adding appropriate weight percent of Nd_2O_3/SrO additions in ZST ceramics could effectively increase the sintered density, permittivity, and quality factor, while reducing the sintering temperature. The sintered ceramics were fully densified at 1320 °C with well-developed grains, homogeneous microstructures and low porosity. Proper ball milling time could significantly improve dielectric performances of ZST ceramics. ZST specimens (milling for 16 h) doped with 0.3 wt% Nd_2O_3 + 0.45 wt% SrO additions sintered at 1320 °C for 4 h displayed the optimal synthetical performances: ε_r = 40.61, Q × f = 40,700 GHz (f = 5.5 GHz) and τ_f = − 2.57 ppm °C^{-1}, which are probably to be promising option for microwave applications.

Acknowledgements The authors are grateful to the support of this work by the Priority Academic Program Development of Jiangsu Higher Education Institutions (PAPD). Jiangsu Collaborative Innovation Center for Advanced Inorganic Function Composites.

References

1. H.C. Xiang, C.C. Li, C.Z. Yin et al., Ceram. Int. **44**(5), 5817 (2018)
2. Y.J. Lin, S.F. Wang, B.C. Lai et al., J. Eur. Ceram. Soc. **37**(8), 2825 (2017)
3. F. Liang, M. Ni, W.Z. Lu et al., J. Alloys Compd. **568**, 11 (2013)
4. Y. Cheng, R.Z. Zuo, Y. Lv, Ceram. Int. **39**(8), 8681 (2013)
5. Y. Wu, D. Zhou, J. Guo et al., Mater. Lett. **65**(17–18), 2680 (2011)
6. Q.W. Liao, L.X. Li, X. Ren et al., J. Am. Ceram. Soc. **95**(11), 3363 (2012)
7. W.T. Xie, H.Q. Zhou, H.K. Zhu et al., J. Mater. Sci. Mater. Electron. **26**(6), 3515 (2015)
8. A. Feteira, D. Iddles, T. Price et al., J. Am. Ceram. Soc. **94**, 817 (2011)

9. S.M. Olhero, A. Kaushal, J.M.F. Ferreira, RSC Adv. **4**(89), 48734 (2014)
10. S. Vahabzadeh, M.A. Golozar, F. Ashrafizadeh, J. Alloys Compd. **509**, 1129 (2011)
11. D. Pamu, G.L.N. Rao, K.V. Saravanan et al., Integr. Ferroelectr. **117**, 118 (2010)
12. C.L. Huang, C.S. Hsu, R.J. Lin, Mater. Res. Bull. **36**, 1985 (2001)
13. D. Pamu, G.L.N. Rao, K.C.J. Raju, J. Alloys Compd. **475**(1–2), 745 (2009)
14. B. Chen, L. Han, B.Y. Li et al., J. Mater. Sci. Mater. Electron. **28**(13), 9542 (2017)
15. S.X. Zhang, J.B. Li, H.Z. Zhai et al., Mater. Chem. Phys. **77**(2), 470 (2002)
16. Q.L. Sun, H.Q. Zhou, X.F. Luo et al., Ceram. Int. **42**(10), 12306 (2016)
17. X.R. Zhang, G.F. Fan, X.H. Wang et al., Ceram. Int. **42**(7), 7962 (2016)
18. Y.S. Ahn, K.H. Yoon, E.S. Kim, J. Eur. Ceram. Soc. **23**(14), 2519 (2003)
19. G.A. Ravi, F. Azough, R. Freer et al., J. Am. Ceram. Soc. **90**, 3947 (2007)
20. H.S. Zhu, Z.Y. Cui, C.Y. Shen, J. Mater. Sci. Mater. Electron. **27**(1), 177 (2016)
21. J.M. Li, Z.H. Tian, L.C. Yao et al., Ceram. Int. **43**(17), 15793 (2017)
22. L.J. Cheng, S.W. Jiang, Q. Ma et al., Scr. Mater. **115**, 80 (2016)
23. R.Z. Zuo, J. Zhang, J. Song et al., J. Am. Ceram. Soc. **101**(2), 569 (2018)
24. W.T. Xie, H.Q. Zhou, H.K. Zhu et al., Ceram. Int. **40**(5), 6899 (2014)
25. R.D. Shannon, J. Appl. Phys. **73**(1), 34 (1993)
26. Y.J. Gu, C. Li, J.L. Huang et al., J. Eur. Ceram. Soc. **37**(15), 4673 (2017)
27. C.L. Huang, M.H. Weng, H.L. Chen, Mater. Chem. Phys. **71**(1), 17 (2001)
28. R.K. Bhuyan, T.S. Kumar, D. Goswami et al., J. Electroceram. **31**(1–2), 48 (2013)
29. S. Takahashi, A. Kan, H. Ogawa, Mater. Chem. Phys. **200**, 257 (2017)
30. L.C. Ren, X.F. Luo, J. Am. Ceram. Soc. **101**(9), 3874 (2018)
31. R. Laishram, O.P. Thakur, J. Mater. Sci. Mater. Electron. **24**(9), 3504 (2013)
32. C.Y. Tsao, K.C. Feng, W.H. Tuan, Ceram. Int. **43**, S312 (2017)